S. Mohammad Amjadi, Mahbub Hoque,
and Kamal Sarabandi

An Iterative Array Signal Segregation Algorithm

A method for interference cancelation and multipath mitigation in complex environments.

IMAGE LICENSED BY INGRAM PUBLISHING

Digital Object Identifier 10.1109/MAP.2016.2630034
Date of publication: 18 April 2017

A frequency-domain array signal segregation using an iterative approach (ASSIA) is developed to estimate the directions of arrival (DoAs), magnitudes, and phases of the signals' spectral components in a multipath environment. This is accomplished by using a uniform circular antenna array whose elements are individually connected to the radio-frequency (RF) front end of a neoteric radio. This technique is utilized to spatially and spectrally separate the communication signals of interest from the strong interfering signals without a priori knowledge regarding their DoAs. Through an extensive comparison with the other techniques reported in the literature, it is shown that ASSIA can detect the DoAs and signal levels of wide dynamic range (DR) much more accurately than what can be done with the existing techniques, provided that the signals' angular spacing is larger than the array beamwidth. Array calibration to capture the fabrication errors is essential to achieve the high level of the DR of signals that ASSIA can handle. The performance of the algorithm in the presence of strong jammers in complex multipath environments with Rayleigh fading characteristics is examined using numerical simulations based on an accurate ray-tracing propagation model. A statistical analysis based on Monte Carlo simulations shows that in such an environment, an ASSIA radio with a 12-element uniform circular

array can improve the signal-to-jammer ratio (SJR) from −20 to at least +2 dB (minimum of 22-dB improvement) in more than 70% of occasions.

INTERFERENCE CANCELATION METHODS

Wireless communication links can be significantly disrupted by stationary or portable smart jammers or unintentional interferers. To resolve this problem, effective jamming cancelation techniques have been extensively examined for the last few decades. Early attempts focused on the method of antenna null steering in the direction of a jammer. A patent based on this concept was filed in 1959 by Paul W. Howells for radar applications [1]. The idea was further explored by Sidney Applebaum, who led the foundation for establishing the concept of adaptive arrays for maximizing the signal-to-interference ratio in time-varying environments in 1965. However, his work was not published until 1976 [2]. Since then, a variety of adaptive beamforming techniques have been conceived [3]–[10]. Applebaum assumes there is only one DoA for the desired signal, and this direction is known. It is also assumed that the statistics (covariance matrix) of the interfering signals are known by the receiver (Rx). To relax the latter requirement, Frost developed another algorithm [11] in which a correcting phase is applied to array elements to focus the beam in the known DoA of the desired signal and optimize the magnitude weighting factors to minimize the total received power. Again, the Frost method assumes a single known DoA and ignores the fact that by minimizing the total received power, the contribution from the desired signal may also be significantly reduced.

Duvall et al. introduced another method [12] to improve upon the Frost algorithm to ensure the desired signal is not significantly reduced when minimizing the total received power. Duvall et al. form a fictitious array composed of pairs of the original array in such a way that the new array elements (adjacent pairs) have a null in the direction of the desired signal. Then, they minimize the total received power of the fictitious array. This way, the desired signal is not entered into the equations. As mentioned, interference mitigation by the Applebaum, Frost, or Duvall methods is accomplished based on three key assumptions.

1) The desired signal arrives from a single direction.
2) The direction of the desired signal is known.
3) The jammer signal and the desired signals are uncorrelated.

The third limitation has been relaxed in the literature by using spatial smoothing techniques [13]–[15]. In another effort, a new beamformer based on the Duvall approach is reported in [16] to cancel out $M-1$ coherent jamming signals by using a 2M-element array. This method still assumes a single DoA for the desired signal and requires this direction to be known. For realistic scenarios pertaining to complex multipath environments in which a large number of the desired and jamming signals of different levels arrive from different unknown directions, neither of these assumptions holds true. Hence, any proposed beamforming method needs to be accompanied by a DoA estimator to discern the DoA of the desired signal.

The traditional eigenstructure-based direction-finding techniques such as multiple signal classification (MUSIC) [17]–[24] or estimation of signal parameters via rotational invariance technique (ESPRIT) [25]–[30] cannot estimate DoAs of fully correlated signals. A spatial-smoothing preprocessing scheme [31] and its improved version [32] are conceived to distinguish the DoA of coherent signals. In [33], the capability of the spatial-smoothing method is further enhanced by using a set of forward and complex conjugate backward subarrays simultaneously, and, hence, the number of identifiable DoAs of coherent signals is increased. A preprocessing conjugate gradient method in combination with a spatial and temporal smoothing technique for DoA estimation of correlated signals is proposed in [35] that exhibits a fast convergence rate. A cumulant-based algorithm [36] and the matrix pencil method (MPM) [37], [38] are used effectively to find the DoAs of coherent signals.

These methods, however, need to have the exact knowledge of the number of the impinging signals on the Rx array for estimation of DoAs. Hence, model-order estimation techniques, such as minimum descriptive length criterion [39] and the Akaike information theoretic criterion [40], [41], are needed to estimate the number of the impinging signals. These methods are based on finding the larger eignenvalues of the data covariance matrix and can be used if the signals are not coherent. In case of coherent (fully correlated) signals, preprocessing techniques such as spatial smoothing or forward–backward averaging [42] have to be run to decorrelate the signals. The forward–backward averaging technique, however, is not able to decorrelate more than two coherent signals.

Although spatial-smoothing techniques [31]–[35] can be used to decorrelate multiple signals, their performance in estimating weak sources is severely affected in the presence of strong interfering sources. Another class of direction-finding techniques is spectral estimation methods, such as minimum variance distortionless response [43], linear prediction [44], and maximum likelihood [45]–[51]. Basically, in spectral estimation methods, the DoAs are found by searching for the local maximums in the spatial spectrum calculated for all directions. These techniques relax the requirement about the a priori knowledge regarding the number of signals.

However, when the DR of the signals arriving from different directions is not small, both eigenstructure-based and spectral estimation methods fail to detect DoAs of the low-level signals. This is a major problem that needs to be addressed, because the desired signals arriving from different directions are usually much smaller than the jamming signals. Also, a difficulty arises when a large number of low-level components of a strong jammer signal arriving from other directions (due to the multipath effect) are comparable to the desired signals. In this case,

these small jamming signals that are correlated with the very large ones must be accurately detected and removed before the desired signals can be retrieved.

In this article, an ASSIA that can be categorized under spectral estimation methods is proposed as an alternative method to the aforementioned techniques for interference cancelation in complex environments. The algorithm provides estimation of the DoAs, magnitudes, and phases of all impinging signals as well as the contribution of each signal at each antenna element without requiring a priori knowledge of the number of DoAs. The algorithm is able to handle a very wide DR of impinging signals compared to the existing techniques provided that the signals are separable by the array (the angular separation of the signals is larger than the adjusted array beamwidth). Because each frequency component is processed individually, both correlated and uncorrelated signals are detected and segregated by ASSIA. By virtue of this algorithm, a radio Rx with two modes of operation including high data rate (HDR) and low data rate (LDR) modes is then proposed to mitigate the interfering signals in a complex multipath environment. The prominent features of the ASSIA radio are 1) it can handle multiple DoAs for the desired signal, 2) it does not require a priori knowledge of DoAs of the desired or interference signals, 3) it does not require the interference signals and the desired signals to be uncorrelated, and 4) for a single stationary source of interference in a multipath environment, the radio is capable of removing the interference in LDR mode even in situations where the DoAs of one or more interference signals are close to those of the desired signal provided that at least one DoA of the interference signal exists that is quite far away from those of the desired signals. The latter feature is achieved due to the capability of ASSIA in estimating the magnitude and phase of all arriving signals, which is not available in other direction-finding and interference-cancelation methods.

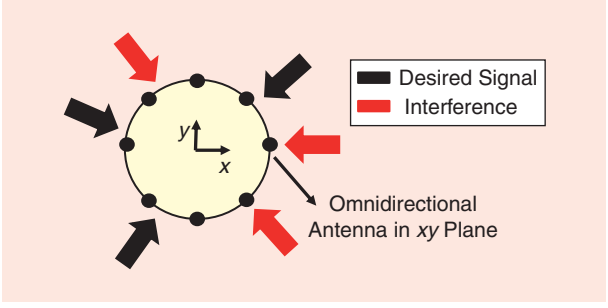

FIGURE 1. A circular array of omnidirectional antennas illuminated by a number of interfering and desired signals.

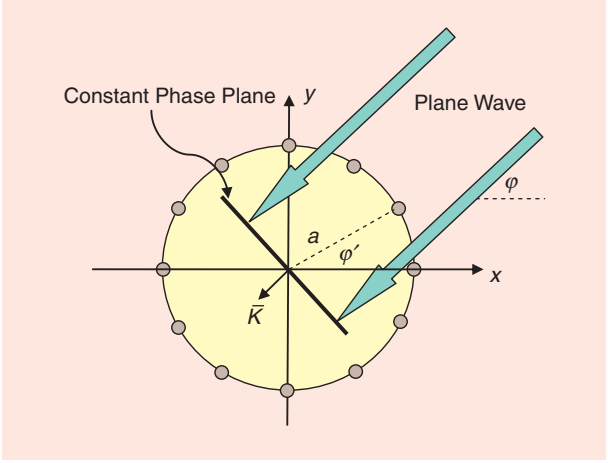

FIGURE 2. The sketch of a uniform circular array illuminated by a plane wave.

ITERATIVE ARRAY SIGNAL SEGREGATION ALGORITHM

PRINCIPLES OF OPERATION

The proposed algorithm is formulized for a two-dimensional case by employing a uniform circular array of omnidirectional antennas as illustrated in Figure 1. The main advantages of the circular array compared to the linear array are its azimuthal symmetry for beamforming without distortion near the end-fire directions as well as the same mutual coupling effect for all antenna elements, which allows for simple coupling mitigation approaches [52]. It is assumed that all the desired and interfering signals are almost confined in the horizontal plane.

As the proposed technique is a frequency-domain method, the received time-domain signal at each antenna is converted to the frequency domain using Fourier transform over a predetermined time interval. The length of the fast Fourier transform (FFT) and the resolution frequency depend on the duration of the time interval the data stream is sampled. Each frequency component is then processed through the ASSIA processor separately to estimate the DoA, magnitude, and phase of the signals. Therefore, irrespective of whether the impinging signals are fully correlated or uncorrelated, ASSIA is able to detect and segregate the signals. After interference detection and removal, the desired signals are converted back to the time domain for further processing. To describe the principle of operation of ASSIA, consider a circular array with radius a, which is illuminated by a number of plane waves as depicted in Figure 2. The number of the Rx antennas and the number of the impinging local plane waves are denoted by M and P, respectively. For simplicity, let us first neglect the mutual coupling among the omnidirectional elements of the array. The antennas are assumed to have a nominal power gain of G and linear vertical polarization. The field expression for each of the incident waves can, locally, be written as $\vec{E} = E_z e^{i\vec{K}\cdot\vec{r}}\hat{z}$, where E_z is the electric field intensity and $\vec{K} = (2\pi f/c)\hat{k} = K\hat{k}$ is the propagation vector. Henceforth, the subscript z in E_z is dropped for simplification. The voltage across each antenna terminal denoted by v_m can then be written as

$$v_m = l_{\text{eff}} E e^{-iKa\cos(\varphi-\varphi_m')}, \tag{1}$$

in which φ and φ_m' are the direction of the impinging plane wave and the angular coordinate of the mth Rx antenna in the polar coordinate system, respectively, and

$$l_{\text{eff}} = \lambda\sqrt{\frac{GR_0}{4\pi\eta_0}}, \tag{2}$$

where λ and η_0 are free space wavelength and intrinsic impedance, respectively, and R_0 is the antenna input impedance. In deriving (1), it is assumed that the antenna is perfectly matched to its input impedance. For P plane waves illuminating the array, the total voltage at the antenna terminals is given by

$$\mathbf{V} = \mathbf{A}(\boldsymbol{\phi})\,\mathbf{E} + \mathbf{N}, \tag{3}$$

where $\mathbf{V}$ is an $M \times 1$ vector of the received voltages,

$$\mathbf{V} = [v_1,\ \ldots, v_M\ ]^T, \tag{4}$$

in which v_m is the total received signal at the mth antenna and $\mathbf{E}$ is a $P \times 1$ vector of the impinging electric fields, and

$$\mathbf{E} = [E_1, \ldots,\ E_P\ ]^T, \tag{5}$$

where E_i is the electric field arriving at the Rx from direction φ_i. $\mathbf{A}(\boldsymbol{\phi})$ is an $M \times P$ matrix of the phase-corrected effective length for the circular antenna array given by

$$\mathbf{A}(\boldsymbol{\phi}) = [a(\varphi_1), \ldots, a(\varphi_P)], \tag{6}$$

where

$$\mathbf{a}(\varphi_p) = \left[l_{\text{eff}}\ e^{-i\,Ka\,\cos(\varphi_p - \varphi_1')}, \ldots, e^{-i\,Ka\,\cos(\varphi_p - \varphi_M')}\right]^T \tag{7}$$

and $\mathbf{N}$ is the noise vector, which is assumed to be a spatially zero-mean white Gaussian process. The goal is to find $\mathbf{E}$ and $\boldsymbol{\phi} = [\varphi_1 \ldots \varphi_P]$ from the total measured received signal denoted by $\mathbf{V}$.

The algorithm is mainly composed of P steps, and each step requires r_s $(1 \le s \le P)$ iterations. As the algorithm proceeds from one step to the next, the number of the detected received signals is increased by one. In other words, at the sth step, the algorithm provides estimations of magnitude and phase of signals arriving from s different directions as a function of frequency. At the very beginning of the sth step, an estimation of the sth largest signal is made. This iteration is defined as the zeroth iteration. Then, the estimations of all s signals are refined through an iterative approach.

At the first step, the algorithm begins with focusing the array in all directions to find the largest arriving signal and its corresponding DoA. An estimation for the DoA of the largest arriving signal denoted by $\varphi_1^{(1,0)}$ is obtained by

$$\varphi_1^{(1,0)} = \underset{\varphi_n}{\text{argmax}}\ (W_n\ V_1^{(1,0)})\ (W_n\ V_1^{(1,0)})^H, \tag{8}$$

where $\mathbf{V_1^{(1,0)}} = \mathbf{V}$ and $\mathbf{W_n}$ is an $M \times 1$ combined focusing and weighting vector to focus the array in direction φ_n with a desired sidelobe level,

$$\mathbf{W_n} = [w_{n1} e^{iKa\,\cos(\varphi_n - \varphi_1')}\ \cdots\ w_{nM} e^{iKa\,\cos(\varphi_n - \varphi_M')}], \tag{9}$$

in which $\varphi_n = n\,\Delta\varphi$ $(n = 1, \ldots, 2\pi/\Delta\varphi)$ and $\Delta\varphi$ is a predetermined search angle step. The superscript H denotes Hermitian transpose. The first and the second superscripts placed in the parentheses in $\varphi_1^{(1,0)}$ and $\mathbf{V_1^{(1,0)}}$ represent the step and the iteration number in that step, respectively. In (9), the phase terms $e^{iKa\,\cos(\varphi_n - \varphi_m')}$ are in fact the conjugate of the phase terms in the phase-corrected effective length $\mathbf{a}(\varphi_n)$ to compensate for the phase difference between Rx antennas to focus the array beam in the direction of φ_n, and $w_{n1}, \ldots, w_{nm}$ are a set of real positive values for M antennas to control the resulting sidelobe level in such a way as to maximize the contribution of the signal coming from direction φ_n and minimize the received signal from other directions. Once $\varphi_1^{(1,0)}$ is found, the zeroth order estimation of the electric field arriving at the Rx from this direction can be obtained from

$$E_1^{(1,0)} = \frac{\mathbf{W_1}\ \mathbf{V_1^{(1,0)}}}{l_{\text{eff}} \sum_{m=1}^{M} w_{1m}}. \tag{10}$$

The summation term in the denominator of (10) is used for normalization. The next step is to estimate the second largest signal E_2 and its DoA φ_2, after which the algorithm improves the estimation accuracy of both E_1 and E_2 as well as φ_1 and φ_2 in an iterative fashion. To find the second largest signal, initially the contribution of the estimated E_1 obtained by (10) is subtracted from the total received signal at each antenna. The result of this subtraction is denoted as $\mathbf{V_2^{(2,0)}}$ and can be found by

$$\mathbf{V_2^{(2,0)}} = \mathbf{V_1^{(1,0)}} - \mathbf{a}\left(\varphi_1^{(1,0)}\right) E_1^{(1,0)}. \tag{11}$$

Thereby, an estimation for the DoA of the second largest signal denoted by $\varphi_2^{(2,0)}$ is found as

$$\varphi_2^{(2,0)} = \underset{\varphi_n}{\text{argmax}}\ (\mathbf{W_n}\ \mathbf{V_2^{(2,0)}})\ (\mathbf{W_n}\ \mathbf{V_2^{(2,0)}})^H, \tag{12}$$

and, consequently, the zeroth order estimation of the second largest signal is given by

$$E_2^{(2,0)} = \frac{\mathbf{W_2}\ \mathbf{V_2^{(2,0)}}}{l_{\text{eff}} \sum_{m=1}^{M} w_{2m}}. \tag{13}$$

The algorithm then proceeds to the first iteration of the second step, in which the estimation of the two largest signals is refined. Because the initial estimations of E_2 and φ_2 are now available, one can improve the estimation accuracy of E_1 and φ_1 by subtracting the contribution of E_2 from all antennas and again trying to find a new estimation for the DoA of the largest signal, which is found by

$$\varphi_1^{(2,1)} = \underset{\varphi_n}{\text{argmax}}\ (\mathbf{W_n}\ \mathbf{V_1^{(2,1)}})\ (\mathbf{W_n}\ \mathbf{V_1^{(2,1)}})^H, \tag{14}$$

where

$$\mathbf{V_1^{(2,1)}} = \mathbf{V_1^{(1,0)}} - \mathbf{a}\left(\varphi_2^{(2,0)}\right) E_2^{(2,0)}. \tag{15}$$

An improved estimation of E_1 is then obtained as

$$E_1^{(2,1)} = \frac{\mathbf{W_1}\ \mathbf{V_1^{(2,1)}}}{l_{\text{eff}} \sum_{m=1}^{M} w_{1m}}. \tag{16}$$

Afterward, E_2 can be updated similarly, that is, the contribution of E_1 is subtracted from the total received signal, and the array pattern is focused in all possible directions to find an update value for E_2 as well as its DoA. This procedure is repeated in the next iterations of the second step until the sequence converges to a solution for E_1 and E_2 as well as φ_1 and φ_2. The algorithm then proceeds to the next step, whereby the third largest signal is first detected. While the contributions of the updated E_1 and E_2 are subtracted from the total received signal, the array beam sweeps the space to find the third largest signal. Then, similar to the second step, the algorithm runs through multiple iterations to refine the estimations of the three largest signals. This procedure is continued in the next steps to estimate all impinging signals that are well above the noise level. Simulations show that the algorithm can handle signals with signal-to-noise ratio (SNR) as low as 5 dB. This is a threshold at which the algorithm is aborted. As the number of the iterations in each step is increased, this iterative approach provides a sequence of improving estimated solutions for $\mathbf{E}$ and $\boldsymbol{\phi}$, which converge eventually. The search angle step, $\Delta\varphi$, needs to be locally decreased around the estimated DoAs over steps and iterations to reduce possible arithmetic errors if the actual DoAs are not among the predetermined search angles. To increase the convergence speed, each signal is estimated using the most updated values of the other signals including those that have been updated within the same iteration. The total number of iterations for each signal depends on the relative magnitude of the signal compared to other signals and the total number of the impinging signals. The larger the estimated signal compared to the other signals and the higher the number of the signals, the higher the number of the iterations the signal goes through. If one defines N_I^s as the number of iterations required to estimate the sth largest signal, then N_I^s is determined by

$$N_I^s = \sum_{i=s}^{P} r_i, \tag{17}$$

where r_i denotes the number of the required iterations in the ith step to make the sequence of the solutions convergent. It is also evident that $E_s^{(i,k)} = 0$ for $i < s$.

The technique is able to detect all signals, provided that the angular separation between two vicinal signals is larger than the array beamwidth. If two or multiple impinging signals are in close angular proximity (smaller than the adjusted array beamwidth), the algorithm fails to segregate them. In this case, the detected signal is the resultant of that set of adjoining signals.

The DR of the signals that the ASSIA radio is able to detect is limited by the DR of the RF amplifiers that can be enhanced by using an automatic gain control and the mixer nonlinearities for large signals (the upper end) and by the Rx noise figure and bandwidth for small signals (the bottom end). The analog-to-digital converter should also be able to provide the required DR and quantization resolution.

MUTUAL COUPLING CONSIDERATIONS

The equations used in the segregation algorithm presented in the previous section ignored the mutual coupling effects among the array elements. To account for the mutual coupling, the weighting coefficients must be modified so that the array can correctly focus in the desired directions. It is also important to mention that the mutual couplings among the antenna elements change the radiation pattern of the elements. That is, the radiation pattern of the elements is no longer omnidirectional. To modify the equations, $\mathbf{W_n}$ is replaced by $\mathbf{W_n^C}$ for a desired radiation pattern having φ_n as its maximum direction of radiation. The synthesis technique for calculating $\mathbf{W_n^C}$ is described in the "Array Weighting Factor Synthesis" section. Assuming that the realized power gain and phase pattern of the mth antenna in the presence of other antennas and the Rx platform are represented as $G_m(\varphi)$ and $P_m(\varphi)$ with reference to the center of the circle, respectively, then, (3) is modified as

$$\mathbf{V} = \mathbf{B}(\boldsymbol{\phi})\,\mathbf{E} + \mathbf{N}, \tag{18}$$

where

$$\mathbf{B}(\boldsymbol{\phi}) = [\mathbf{b}(\varphi_1), \ldots, \mathbf{b}(\varphi_P)], \tag{19}$$

and

$$\mathbf{b}(\varphi_p) = [l_{\text{eff},1}(\varphi_p) \ldots l_{\text{eff},M}(\varphi_p)]^T, \tag{20}$$

where

$$l_{\text{eff},m}(\varphi_p) = \lambda \sqrt{\frac{G_m(\varphi_p)\, R_0}{4\pi\eta_0}}\; e^{iP_m(\varphi_p)}. \tag{21}$$

Consequently, the equations in the zeroth iteration of the first step take the following forms:

$$\varphi_1^{(1,0)} = \underset{\varphi_n}{\text{argmax}}\; (\mathbf{W_n^C}\,\mathbf{V_1^{(1,0)}})\,(\mathbf{W_n^C}\,\mathbf{V_1^{(1,0)}})^H, \tag{22}$$

where

$$\mathbf{W_n^C} = [w_{n1}^C \ldots w_{nm}^C], \tag{23}$$

and

$$E_1^{(1,0)} = \frac{\mathbf{W_1^C}\,\mathbf{V_1^{(1,0)}}}{\sum_{m=1}^{N_A} w_{1m}^C l_{\text{eff},m}\left(\varphi_1^{(1,0)}\right)}. \tag{24}$$

Also, the equations in the zeroth iteration of the second step are modified as follows:

$$\mathbf{V_2^{(2,0)}} = \mathbf{V_1^{(1,0)}} - \mathbf{b}\left(\varphi_1^{(1,0)}\right) E_1^{(1,0)}, \tag{25}$$

$$\varphi_2^{(2,0)} = \underset{\varphi_n}{\text{argmax}}\; (\mathbf{W_n^C}\,\mathbf{V_2^{(2,0)}})\,(\mathbf{W_n^C}\,\mathbf{V_2^{(2,0)}})^H, \tag{26}$$

and

$$E_2^{(2,0)} = \frac{\mathbf{W_2^C}\,\mathbf{V_2^{(2,0)}}}{\sum_{m=1}^{M} w_{2m}^C l_{\text{eff},m}\left(\varphi_2^{(2,0)}\right)}. \tag{27}$$

Similarly, the equations pertaining to other steps and iterations are modified. It should be noted that $l_{\text{eff},m}(\varphi)$ can be obtained by either full-wave simulation or measurement. The sequence through which the algorithm runs is demonstrated in Table 1. The approach that is used to calculate $\mathbf{W_n^C}$ is discussed next.

TABLE 1. THE SUMMARY OF ASSIA.

Step Number (p)	Iteration Number (k)	Descriptions						
1	0	$E_1^{(1,0)}$	The first estimation of E_1 is made.					
2	0	$E_2^{(2,0)}$	The first estimation of E_2 is made.					
	1	$E_1^{(2,1)}$	$E_2^{(2,1)}$	In each iteration, the signals are calculated from the largest $E_1^{(p,k)}$ to the smallest $E_p^{(p,k)}$ sequentially ($1 \le k \le r_p$, $1 \le s \le p$). $\varphi_s^{(2,k)} = \underset{\varphi_n}{\text{argmax}} \left(\mathbf{W}_n^C \mathbf{V}_s^{(2,k)}\right) \left(\mathbf{W}_n^C \mathbf{V}_s^{(2,k)}\right)^H$				
	⋮	⋮	⋮	$E_s^{(2,k)} = \dfrac{\mathbf{W}_s^C \mathbf{V}_s^{(2,k)}}{\sum_{m=1}^{M} w_{\text{sm}}^C I_{\text{eff},m}(\varphi_s^{(2,k)})}$				
	r_2	$E_1^{(2,r_2)}$	$E_2^{(2,r_2)}$	$\mathbf{V}_s^{(2,k)} = \mathbf{V}_1^{(1,0)} - \sum_{q=1}^{s-1} \mathbf{b}(\varphi_q^{(2,k)})\, E_q^{(2,k)} + \sum_{q=s+1}^{2} \mathbf{b}(\varphi_q^{(2,k-1)})\, E_q^{(2,k-1)}$				
3	0	$E_3^{(3,0)}$	The first estimation of E_3 is made.					
	1	$E_1^{(3,1)}$	$E_2^{(3,1)}$	$E_3^{(3,1)}$	$\varphi_s^{(3,k)} = \underset{\varphi_n}{\text{argmax}} \left(\mathbf{W}_n^C \mathbf{V}_s^{(3,k)}\right) \left(\mathbf{W}_n^C \mathbf{V}_s^{(3,k)}\right)^H$			
	⋮	⋮	⋮	⋮ $E_3^{(3,r_3)}$	$E_s^{(3,k)} = \dfrac{\mathbf{W}_s^C \mathbf{V}_s^{(3,k)}}{\sum_{m=1}^{M} w_{\text{sm}}^C I_{\text{eff},m}(\varphi_s^{(3,k)})}$			
	r_3	$E_1^{(3,r_3)}$	$E_2^{(3,r_3)}$		$\mathbf{V}_s^{(3,k)} = \mathbf{V}_1^{(1,0)} - \sum_{q=1}^{s-1} \mathbf{b}(\varphi_q^{(3,k)})\, E_q^{(3,k)} + \sum_{q=s+1}^{3} \mathbf{b}(\varphi_q^{(3,k-1)})\, E_q^{(3,k-1)}$			
⋮	⋮	⋮	⋮	⋮	⋮	⋮	⋮	⋮
P	0	$E_P^{(P,0)}$	The first estimation of E_P is made.					
	1	$E_1^{(P,1)}$	$E_2^{(P,1)}$	$E_3^{(P,1)}$	$E_4^{(P,1)}$		$E_P^{(P,1)}$	$\varphi_s^{(P,k)} = \underset{\varphi_n}{\text{argmax}} \left(\mathbf{W}_n^C \mathbf{V}_s^{(P,k)}\right) \left(\mathbf{W}_n^C \mathbf{V}_s^{(P,k)}\right)^H$
	⋮	⋮	⋮	⋮	⋮	…	⋮	$E_s^{(P,k)} = \dfrac{\mathbf{W}_s^C \mathbf{V}_s^{(P,k)}}{\sum_{m=1}^{M} w_{\text{sm}}^C I_{\text{eff},m}(\varphi_s^{(P,k)})}$
	r_P	$E_1^{(P,r_P)}$	$E_2^{(P,r_P)}$	$E_3^{(P,r_P)}$	$E_4^{(P,r_P)}$		$E_P^{(P,r_P)}$	$\mathbf{V}_s^{(P,k)} = \mathbf{V}_1^{(1,0)} - \sum_{q=1}^{s-1} \mathbf{b}(\varphi_q^{(P,k)})\, E_q^{(P,k)} + \sum_{q=s+1}^{P} \mathbf{b}(\varphi_q^{(P,k-1)})\, E_q^{(P,k-1)}$

ARRAY WEIGHTING FACTOR SYNTHESIS

As was described in the "Mutual Coupling Considerations" section, at each iteration, the algorithm goes through a spatial search process over all possible directions. Let's define $l_{\text{eff},m}(\varphi)$ as the effective length of each antenna in the horizontal plane (xy plane) in the presence of all other antennas and the Rx platform with its phase center at the center of the circular array. The effective length of the circular array denoted as $L_{\text{eff}}(\varphi)$ can then be written as

$$L_{\text{eff}}(\varphi) = \sum_{m=1}^{M} w_{nm}^C \, l_{\text{eff},m}(\varphi). \tag{28}$$

Due to the symmetrical nature of a circular array and under the assumption that the array elements are identical and equally spaced, the effective length of each element can be expressed as a spatially shifted function of that of a reference antenna

$$l_{\text{eff},m}(\varphi) = l_{\text{eff},1}\left(\varphi - \frac{2\pi m}{M}\right), \tag{29}$$

where $l_{\text{eff},1}(\varphi)$ is the normalized effective length of the antenna located at $\varphi = \varphi'_1$ with reference to the center of the circle obtained by full-wave simulation or measurement. Substituting (29) in (28), the array effective length takes the form

$$L_{\text{eff}}(\varphi) = \sum_{m=1}^{M} w_{nm}^C \, l_{\text{eff},1}\left(\varphi - \frac{2\pi m}{M}\right). \tag{30}$$

Representing $L_{\text{eff},n}(\varphi)$ and $l_{\text{eff},1}(\varphi - 2\pi m/M)$ in the Fourier series and substituting in (28) results in

$$\sum_{k=-\infty}^{+\infty} a_k e^{ik\varphi} = \sum_{m=1}^{M} w_{nm}^{C}\left(\sum_{k=-\infty}^{+\infty} b_k e^{-ik\frac{2\pi m}{M}} e^{ik\varphi}\right), \tag{31}$$

in which

$$a_k = \frac{1}{2\pi}\int_0^{2\pi} L_{\text{eff},n}(\varphi)\, e^{-ik\varphi}\, d\varphi, \text{ and} \tag{32}$$

$$b_k = \frac{1}{2\pi}\int_0^{2\pi} l_{\text{eff},1}\, e^{-ik\varphi}\, d\varphi. \tag{33}$$

Interchanging the summations in the right-hand side of (31), it can be rewritten as

$$\sum_{k=-\infty}^{+\infty} a_k e^{ik\varphi} = \sum_{k=-\infty}^{+\infty} b_k\, e^{ik\varphi}\left(\sum_{m=1}^{M} w_{nm}^{C}\, e^{-ik\frac{2\pi m}{M}}\right). \tag{34}$$

For (34) to be valid for all values of φ, we must have

$$a_k e^{ik\varphi} = b_k\, e^{ik\varphi} \sum_{m=1}^{M} w_{nm}^{C}\, e^{-ik\frac{2\pi m}{M}}, \tag{35}$$

which can be used to find a_k:

$$a_k = b_k \sum_{n=1}^{M} w_{nm}^{C}\, e^{-ik\frac{2\pi m}{M}}. \tag{36}$$

When defining

$$g(k) = \frac{a_k}{b_k} = \sum_{m=1}^{M} w_{nm}^{C}\, e^{-ik\frac{2\pi m}{M}}, \tag{37}$$

$g(k)$ can be viewed as a truncated finite Fourier series, and, therefore, the weighing factors can be obtained from

$$w_{nm}^{C} = \frac{1}{M}\sum_{k=-\infty}^{+\infty} g(k)\, e^{ik\frac{2\pi m}{M}}. \tag{38}$$

Using (32) and (33) in (38),

$$w_{nm}^{C} = \frac{1}{M}\sum_{k=-\infty}^{+\infty}\left[\frac{\int_0^{2\pi} L_{\text{eff}}(\varphi)\, e^{-ik\varphi}\, d\varphi}{\int_0^{2\pi} l_{\text{eff},1}\, e^{-ik\varphi}\, d\varphi}\right] e^{ik\frac{2\pi m}{M}}. \tag{39}$$

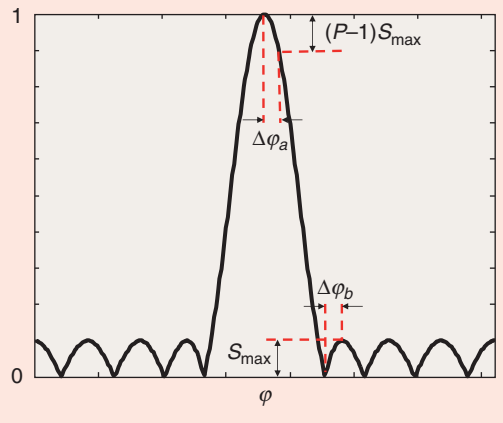

FIGURE 3. The normalized effective length of the array given by (40). The condition $\Delta\varphi_b > \Delta\varphi_a$ is necessary for the convergence of the algorithm.

The combined focusing and weighting vector, $\mathbf{W}_n^C$, is provided in (39) in an equally spaced circular array of M elements for the desired radiation pattern $L_{\text{eff}}(\varphi)$. In this article, a realizable Dolph–Chebyshev function for the normalized effective length of the array, $L_{\text{eff}}(\varphi)$, is used, which is defined as [53]

$$L_{\text{eff}}(\varphi) = \cosh\left(2h\, \cosh^{-1}\left(z_0 \cos\left(\frac{\varphi-\varphi_n}{2}\right)\right)\right). \tag{40}$$

In (40), φ_n represents the direction of the look angle, and z_0 defines the sidelobe level through the following equation:

$$z_0 = \cosh\left(\frac{1}{2h}\cosh^{-1}\left(\frac{1}{S_{\max}}\right)\right). \tag{41}$$

Here, $S_{\max}$ is the ratio of the sidelobe level to the main lobe level, and h is a number satisfying the following condition:

$$h \le \frac{M-1}{2}. \tag{42}$$

CONVERGENCE ANALYSIS

The sufficient condition under which the sequence of the solutions generated by the algorithm converges to the correct solution is examined in this section. The error in the detected magnitude of the largest signal denoted by $\left|err_{E_1}^{(1,0)}\right|$ is given by

$$\left|err_{E_1}^{(1,0)}\right| = \left|\sum_{n=2}^{P} S(\varphi_n)E_n + \gamma_1^{(1,0)}\left(\sum_{n=2}^{P} S(\varphi_n)E_n\right)\right|. \tag{43}$$

The first term represents the contribution from other signals through sidelobes, and the second term refers to the error in the estimation of $|E_1|$ that is generated due to the error in the estimation of φ_1. The second term, however, is a function of the first term and can be approximated by

$$\gamma_1^{(1,0)}(\alpha) \cong \sum_{n=2}^{P} S_{\max} E_n - \alpha, \tag{44}$$

where $S_{\max} = \max(S(\varphi))$ is the maximum sidelobe level of the array that can be obtained from (40) (see Figure 3). In (44), the parameter α is defined as $\alpha = \sum_{n=2}^{P} S(\varphi_n)E_n$, and, in the worst case, α takes its maximum value when all other signals happen to be in the directions of maximum sidelobes and add up coherently as the array is focused in the direction φ_1. In this case, the error in the detection of φ_1 is equal to zero, which in turn results in $\gamma_1^{(1,0)}(\alpha_{\max}) = 0$. On the other hand, the minimum value of α occurs when all other signals happen to be at the directions of the array nulls. Here, the direction of look is different from φ_1, and the error in the estimation of φ_1 is maximum. This implies that, as the first term in the right-hand side of (43) increases, the second term decreases and vice versa. Therefore, to ensure the convergence of the algorithm, both types of errors, that is, the error in the estimation of DoAs and the error in the estimation of magnitudes and phases of the signals, should be decreased simultaneously as the number of the iterations

is increased. As was described in the "Iterative Array Signal Segregation Algorithm" section, the algorithm is based on subtracting the contribution of the estimated larger signals and then searching for the smaller ones. This procedure can be viewed as creating nulls in the directions of the detected signals while looking for the others. To reduce the error in the location of the created nulls in each iteration, the maximum error in the estimation of φ_1 denoted by $\Delta\varphi_a$ resulting from the maximum variation of α should be smaller than the smallest angular distance between two adjacent peaks and nulls of the array sidelobes denoted by $\Delta\varphi_b$. The reason is that the maximum error occurs when the created null happens to be in the direction of one of the array nulls. The worst case corresponds to coherent and equal magnitude signals. With reference to Figure 3, the necessary condition for which the error in the estimation of DoAs is reduced iteratively is

$$\Delta\varphi_b > \Delta\varphi_a. \tag{45}$$

For the array effective length given by (40), it can be shown that condition (45) translates to

$$\cos^{-1}\left[\frac{1}{z_0}\cos\left(\frac{3\pi}{4h}\right)\right]-\cos^{-1}\left[\frac{1}{z_0}\cos\left(\frac{\pi}{4h}\right)\right] > 2\cos^{-1}\left[\frac{1}{z_0}\cosh\left(\frac{1}{2h}\cosh^{-1}(a_0-R)\right)\right], \tag{46}$$

where

$$a_0 = \cosh\left(\frac{1}{2h}\cosh^{-1}\left(\frac{1}{S_{\max}}\right)\right) \tag{47}$$

and

$$R = S_{\max}a_0(P-1). \tag{48}$$

The sufficient condition for convergence is not, however, in (45). As was mentioned previously, the error in the estimation of the magnitude and phase of the signals should also be decreased iteratively. Starting with the first step of the algorithm and substituting (44) in (43), it is concluded that

$$\left|err_{E_1}^{(1,0)}\right| \le \sum_{n=2}^{P} |S_{\max}E_n|. \tag{49}$$

In the second step, we have

$$\begin{aligned}|err_{E_2}^{(2,0)}| &\le \left|S(\varphi_n)er_{E_1}^{(1,0)} + \sum_{n=2}^{P} S(\varphi_n)E_n \right. \\ &\quad \left. + \left(S(\varphi_n)er_{E_1}^{(1,0)} + \sum_{n=2}^{P} S(\varphi_n)E_n\right)\right| \\ &\le \left|S_{\max}er_{E_1}^{(1,0)}\right| + \sum_{n=2}^{P} |S_{\max}E_n|,\end{aligned} \tag{50}$$

where

$$\gamma_2^{(2,0)}(\alpha) \cong \left|S_{\max}er_{E_1}^{(1,0)}\right| + \sum_{n=2}^{P} |S_{\max}E_n| - \alpha. \tag{51}$$

Similarly, the error in detecting $|E_1|$ in each iteration of the second step is given by

$$\begin{aligned}\left|er_{E_1}^{(2,k)}\right| &\le |S_{\max}er_{E_2}^{(2,k-1)}| + \sum_{p=3}^{P} |S_{\max}E_n| = \\ &|S_{\max}^{k+2}E_2| + \sum_{n=3}^{P}\left|\sum_{n=1}^{k+2} S_{\max}^{n}E_n\right| = |S_{\max}^{k+2}E_2| + \sum_{n=3}^{P}\left|\frac{S_{\max}}{1-S_{\max}}E_n\right|.\end{aligned} \tag{52}$$

In the limit, when the number of the iterations is large enough, the error asymptotically approaches

$$\lim_{k\to\infty}\left|er_{E_1}^{(2,k)}\right| = \sum_{n=3}^{P}\left|\frac{S_{\max}}{1-S_{\max}}E_n\right|. \tag{53}$$

Similarly, for the second largest signal, we have

$$\begin{aligned}|er_{E_2}^{(2,k)}| &\le \left|S_{\max}er_{E_1}^{(2,k-1)}\right| + \sum_{n=3}^{P}|S_{\max}E_n| = |S_{\max}^{k+2}E_1| \\ &\quad + \sum_{n=3}^{P}\left|\sum_{q=1}^{k+2} S_{\max}^{q}E_n\right| \le |S_{\max}^{k+2}E_1| + \sum_{n=3}^{P}\left|\frac{S_{\max}}{1-S_{\max}}E_n\right|\end{aligned} \tag{54}$$

and

$$\lim_{k\to\infty}|er_{E_2}^{(2,k)}| \le \sum_{n=3}^{P}\left|\frac{S_{\max}}{1-S_{\max}}E_n\right|. \tag{55}$$

Following this procedure and going through a lengthy algebra, it can be shown that, in the last step, the asymptotic error is given by

$$\lim_{k\to\infty}\left|err_{E_1}^{(P,k)}\right| \le \lim_{k\to\infty}\left\{S_{\max}^{k}\left[(P-1)S_{\max}+(P-2)\right]^{k} \times\left|\frac{S_{\max}}{1-(P-2)S_{\max}}\right||E_P|\right\} \tag{56}$$

$$\lim_{k\to\infty}\left|err_{E_{P-1}}^{(P,k)}\right| \le \lim_{k\to\infty}\left\{S_{\max}^{k}\left[(P-1)S_{\max}+(P-2)\right]^{k} \times\left|\frac{S_{\max}}{1-(P-2)S_{\max}}\right||E_P|\right\}, \tag{57}$$

and

$$\lim_{k\to\infty}\left|err_{E_P}^{(P,k)}\right| \le \lim_{k\to\infty}\left\{(P-1)S_{\max}^{k+1}\left[(P-1)S_{\max}\ (P-2)\right]^{k+1} \times\left|\frac{S_{\max}}{1-(P-2)S_{\max}}\right||E_P|\right\}. \tag{58}$$

Therefore, an upper bound on $S_{\max}$ should be imposed so that

$$(P-1)\ S_{\max}^{2}+(P-2)S_{\max} < 1, \tag{59}$$

which implies that

$$S_{\max} < \frac{\sqrt{(P-2)^2+4(P-1)}-(P-2)}{2(P-1)}. \tag{60}$$

The sufficient conditions to fulfill the convergence of the algorithm are given in (45) and (60). For a 12-element circular array of diameter $D = 1.44\lambda$, the graph of maximum sidelobe

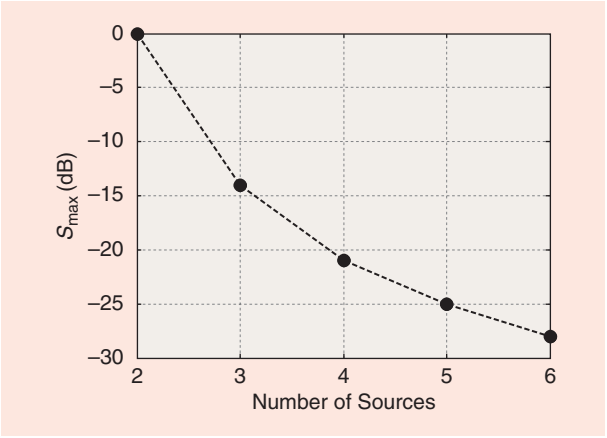

FIGURE 4. The maximum sidelobe level versus number of signals required for convergence for an array with the effective length given by (40).

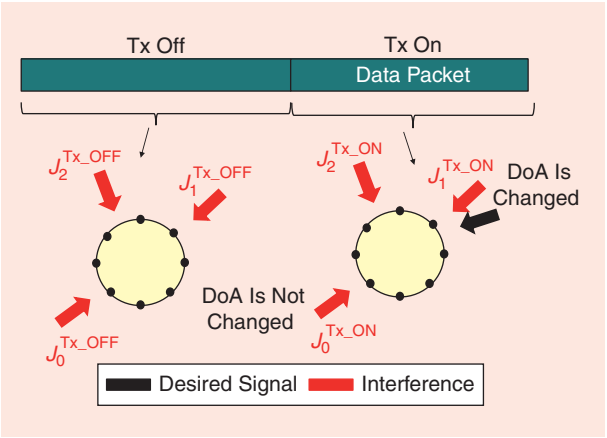

FIGURE 5. The LDR mode, where jammer cancelation is accomplished by turning the Tx on and off with a pattern known to the Rx. The DoAs and levels of the jammer are estimated during the off cycle and used to cancel the jammer signal during the on cycle.

level versus number of coherent signals that satisfies both conditions is given in Figure 4.

INTERFERENCE SEGREGATION

After detecting signals from all directions, one needs to discern the desired signals from interference. This can be accomplished by using the training sequence as part of the desired transmitted data stream. The signal, which exhibits a low level of cross-spectral density with the training sequence, is considered as the interfering signal, and its contribution at each antenna is then subtracted from the total received signal at each antenna. Then, using the training sequence as part of the received signal, the channel response from the transmitter (Tx) to each Rx antenna is estimated. Once the channel transfer function is computed, the transmitted data can be retrieved. Smart jammers, however, are able to detect the communication signals and then produce and radiate a corrupted copy of the signals. To avoid this, a directional modulation technique [54], [55] can be utilized at the Tx point to minimize the bite error rate (BER) in the desired Tx-to-Rx channel and to maximize the BER in other directions. By this provision, the jammer will not be able to correctly detect the training sequence and generate a distorted version of the desired signal. The radio link can be designed to work in two different modes, HDR or normal mode and LDR. If the DoAs of the communication signal of interest are not in close angular proximity to the interfering signals, the radio link can work in its normal or HDR mode. For the scenarios in which the DoAs of the desired and interfering signals cannot be resolved by the array beamwidth, interference cancelation is possible in LDR mode. In LDR mode, the Tx operates intermittently with a pattern known to the Rx using synchronized clocks. The off-time duration of the Tx is set to be close to the length of the data packet. When the transmitter is off, the received signal is from the interferer only (see Figure 5), whose DoAs and level are measured by the radio as before. Assuming there is only one jammer present and the channel transfer function does not change during the short interval of a data packet, the interference in directions where DoAs of the signal and jammers are close can be removed. This is done by first identifying small but measureable changes in the levels and DoAs of signals in directions when the Tx was off. These are directions where the desired signal and jammer DoAs are close and not separable. Using a strong jammer signal from a direction not close to the desired signal as reference (J_0 in Figure 5), the jammer signals in directions where the jammer and the desired signal DoAs are close can be estimated accurately and removed. For example, referring to Figure 5, $J_1^{TX\_ON}$ can be obtained from

$$J_1^{TX\_ON}(f) \cong J_0^{TX\_ON}(f)\frac{J_1^{TX\_OFF}(f)}{J_0^{TX\_OFF}(f)}. \tag{61}$$

In view of (61), the ASSIA processor enables the radio Rx to mitigate interference in LDR mode as a result of the inherent feature of the algorithm in terms of estimating the magnitude and phase of all arriving desired and interfering signals, which is not attainable in other direction-finding and interference suppression techniques.

COMPARISON WITH OTHER TECHNIQUES

In this section, the performance characteristics of ASSIA are evaluated in comparison with other techniques using computer simulations, and its convergence behavior is also demonstrated. Initially, a simple scenario is considered to indicate the ability of the proposed algorithm to segregate the DoA as well as the magnitude and phase of a number of monochromatic plane waves impinging an Rx with a circular array. The array is composed of 12 equally spaced dipole antennas with a diameter of $D = 2a = 1.44\,\lambda$. It is also assumed that the array is illuminated by six monochromatic plane waves from different directions. The background noise is neglected in this simulation. The estimated DoAs and magnitudes of the signals versus iteration number are shown in Figures 6 and 7, respectively. It is evident that, in each step, the algorithm converges after a few iterations (fewer than five), denoted by r_s. The total number of iterations

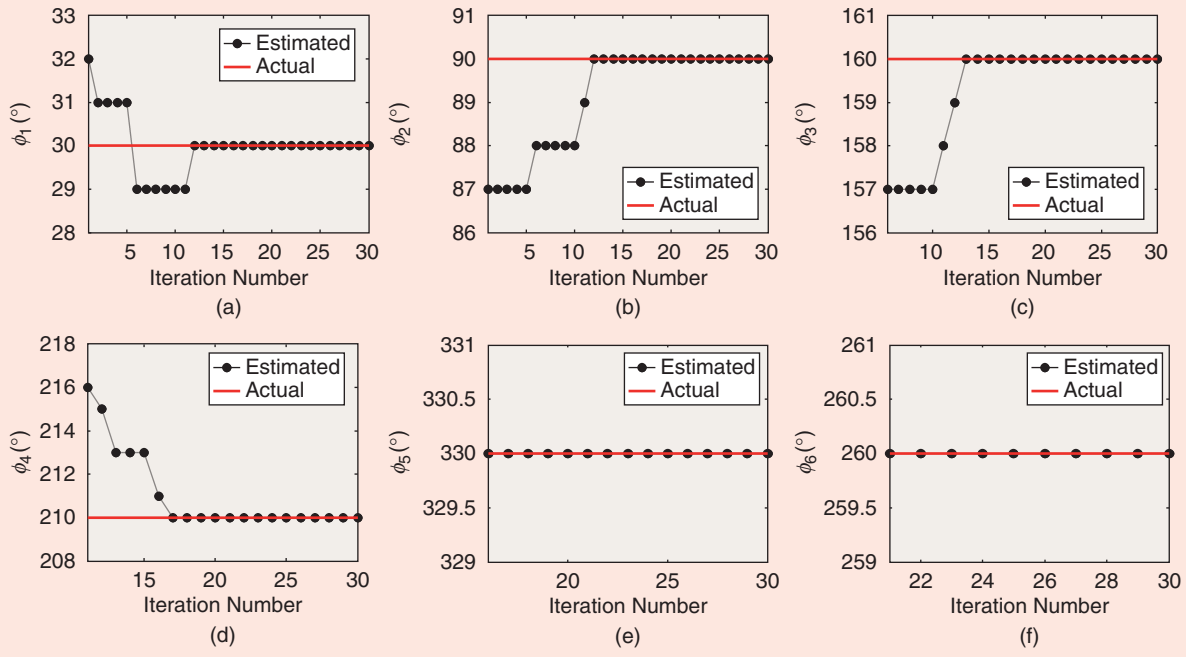

FIGURE 6. The estimated DoAs versus iteration number. The red lines represent the actual, and the symbols denote the estimated values.

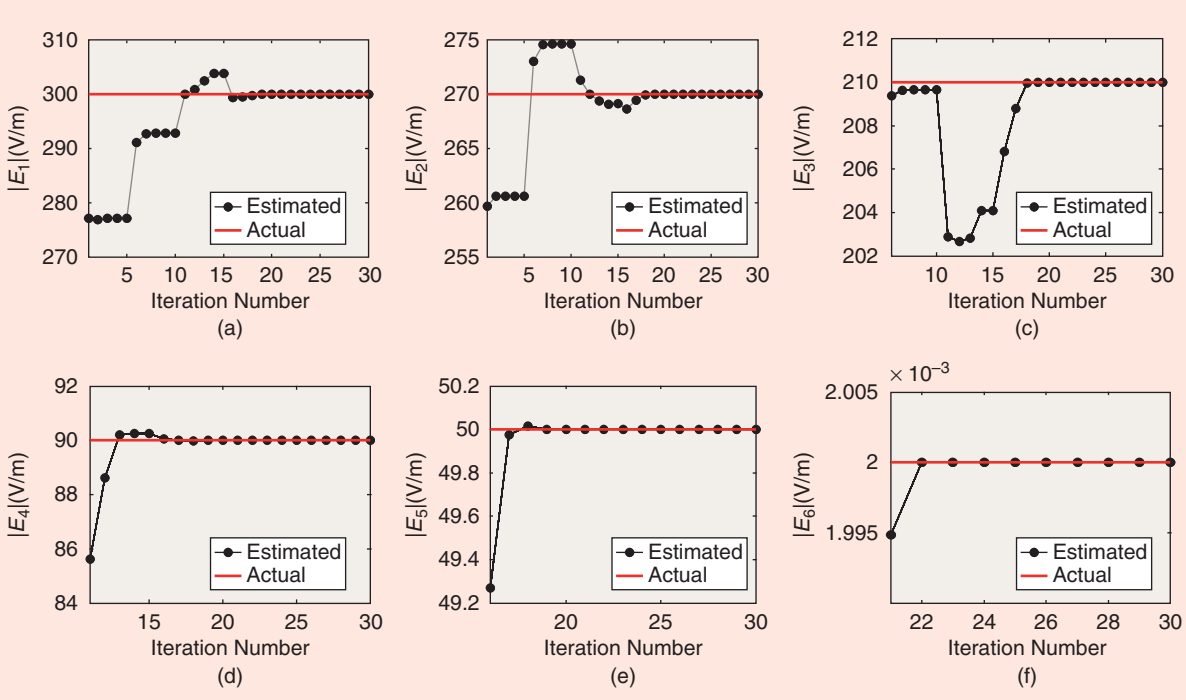

FIGURE 7. (a)–(f) The estimated magnitudes of the signals versus iteration number. The red lines represent the actual, and the symbols denote the estimated values.

to estimate each signal, defined as N_i^s, depends on its magnitude compared to other signals and the total number of impinging signals that are above the threshold level. For the lower-level signals, the convergence is faster. The reason is that the signals are estimated in a descending order and, when it comes to the lower signals, an accurate estimation of the larger ones is already made and their contribution are already subtracted from the total. The range of the horizontal axis in Figures 6 and 7

TABLE 2. THE DOAs AND SNRs FOR THE FOUR-SIGNAL SCENARIO.

Signal Number	DoA	SNR (dB)
1	50°	65
2	140°	60
3	230°	55
4	320°	5–50

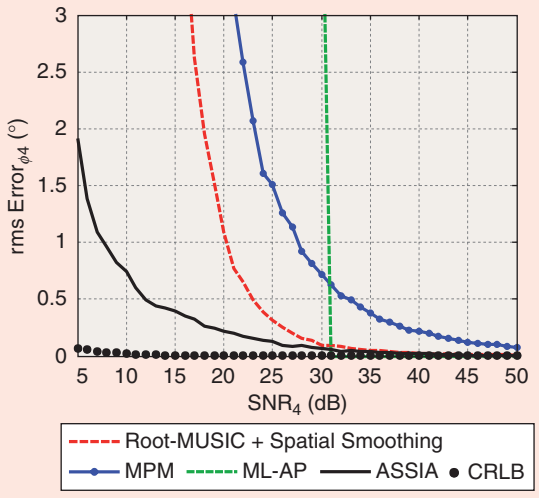

FIGURE 8. The rms error in estimating φ_4 versus SNR_4 using different techniques for the scenario in which four correlated signals of different SNRs listed in Table 2 are impinging on the array. CRLB: Cramér–Rao lower bound.

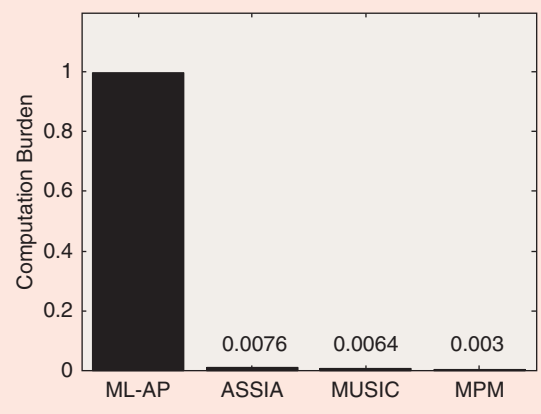

FIGURE 9. The computation burden of ASSIA compared to other methods for the four-signal scenario.

(Itr. no.$_{\max}$ − Itr. no.$_{\min}$) represents N_I^s. As mentioned previously, $E_s^{(i,k)} = 0$ for $i < s$. It can be observed that 100 − dB DR (20 $\log(|E_1/E_6|)$) is handled by this technique using a 12-element circular array of diameter 1.44 λ.

TABLE 3. THE DOAs AND SNRs FOR THE SEVEN-SIGNAL SCENARIO.

Signal Number	DoA	SNR (dB)	Signal Number	DoA	SNR (dB)
1	35°	65	5	290°	65
2	85°	65	6	345°	45
3	140°	40	7	240°	5–65
4	190°	40			

A quantitative comparison with other techniques, including root-MUSIC [18] in conjunction with spatial smoothing [31], the MPM [37], and maximum likelihood by alternating projection (ML-AP) [45], is performed with additive zero-mean white Gaussian noise. To implement root-MUSIC, a transformation to a virtual array [34] is applied to the circular array to make the data matrix amenable to spatial smoothing. This transformation is also used before applying the MPM as it cannot directly be applied to a circular array. The circular array is recommended to have an odd number of elements for efficient performance of this transformation [34]. Therefore, to make a fair comparison, a 15-element circular array of diameter $D = 1.6\ \lambda$ is considered. It is assumed that four fully correlated signals with different SNRs spread over a wide DR are illuminating the array from different directions, as listed in Table 2. The root-mean-square (rms) error in the estimation of the DoA of the source located at $\varphi = \varphi_4$ by varying the SNR of the signal arriving from the fourth direction (SNR_4) while keeping the SNR of the three other signals fixed is calculated and plotted in Figure 8 using different techniques based on 100 Monte Carlo simulations. It should be noted that the same time duration of signals was taken for all techniques. It is observed that ASSIA exhibits superior performance, particularly when SNR_4 is much lower than the other three signals. For this scenario, maximum likelihood fails to converge in detecting φ_4 if the DR denoted by $\text{DR} = \text{SNR}_{\max} - \text{SNR}_4$ is larger than 35 dB. The detection errors of root-MUSIC and the MPM start to increase dramatically for DR > 45 dB and DR > 40 dB, respectively, while ASSIA provides estimation of the DoA of the weakest signal with less than 2° error up to DR = 60 dB and SNR = 5 dB.

The computation time of ASSIA is compared with the other methods for this experiment and is illustrated in Figure 9. The computation time of ASSIA is comparable to MUSIC, 2.5 times more than the MPM, and 130 times less than the maximum likelihood method.

Another factor that affects the performance of DoA estimation techniques is the number of the receiving signals. Using the same Rx array, the performance of ASSIA is evaluated and compared with the other estimators for another scenario in which the number of the receiving signals is increased to seven. The DoAs and SNRs of the signals are listed in Table 3. Performing 100 Monte Carlo runs, the resultant rms error in detecting angle of arrival of the seventh signal (φ_7) by varying the SNR of the signal

arriving from the seventh direction (SNR_7) while keeping the SNR of the six other signals fixed is shown in Figure 10 for different estimators. The performance of root-MUSIC is severely degraded because the effective aperture of the array is substantially reduced after spatial smoothing. It is also evident that the maximum likelihood breaks down in this scenario when $DR = SNR_{max} - SNR_7$ is larger than 10 dB. The reason for the failure of the maximum likelihood is that the dependence of the global convergence on the initialization is very strong in all deterministic or randomized hill-climbing techniques. In case of large DR and a large number of arriving signals, the probability of choosing a good initial point to render the convergence to the correct solution is much less. The resultant rms error for the MPM is much higher than what is achieved by ASSIA, particularly for DR > 20 dB. Compared to the four-signal scenario, it is observed that the estimation error of the MPM is increased, while the estimation error of ASSIA is smaller than 1.5° for SNR = 5 dB and DR = 60 dB.

The keys to the success of ASSIA in situations where the signals' DR is wide and the number of signals arriving from different directions is high are 1) no initialization is required for the signals at the beginning and 2) the signal levels and the DoAs based on estimating and removing the strongest signals are calculated through a multistep iterative approach. In this fashion, the errors are effectively prevented to propagate while moving toward estimating the smaller signals.

The capability of ASSIA in detecting correlated signals over a very wide DR is of great importance for interference

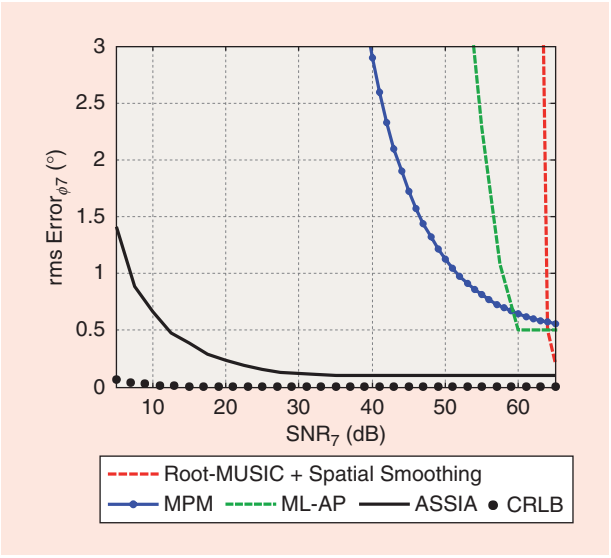

FIGURE 10. The rms error in estimating φ_7 versus SNR_7 using different techniques for the scenario in which seven correlated signals of different SNRs listed in Table 3 are impinging on the array.

cancelation, as, in realistic situations, the level of the interference signal is usually much larger than the desired signal. Moreover, as will be shown later, in complex environments, there exist multiple correlated interference signals and multiple correlated desired signals spanning a wide range of magnitudes arriving at the Rx from different directions. As described before, all adaptive array techniques require the

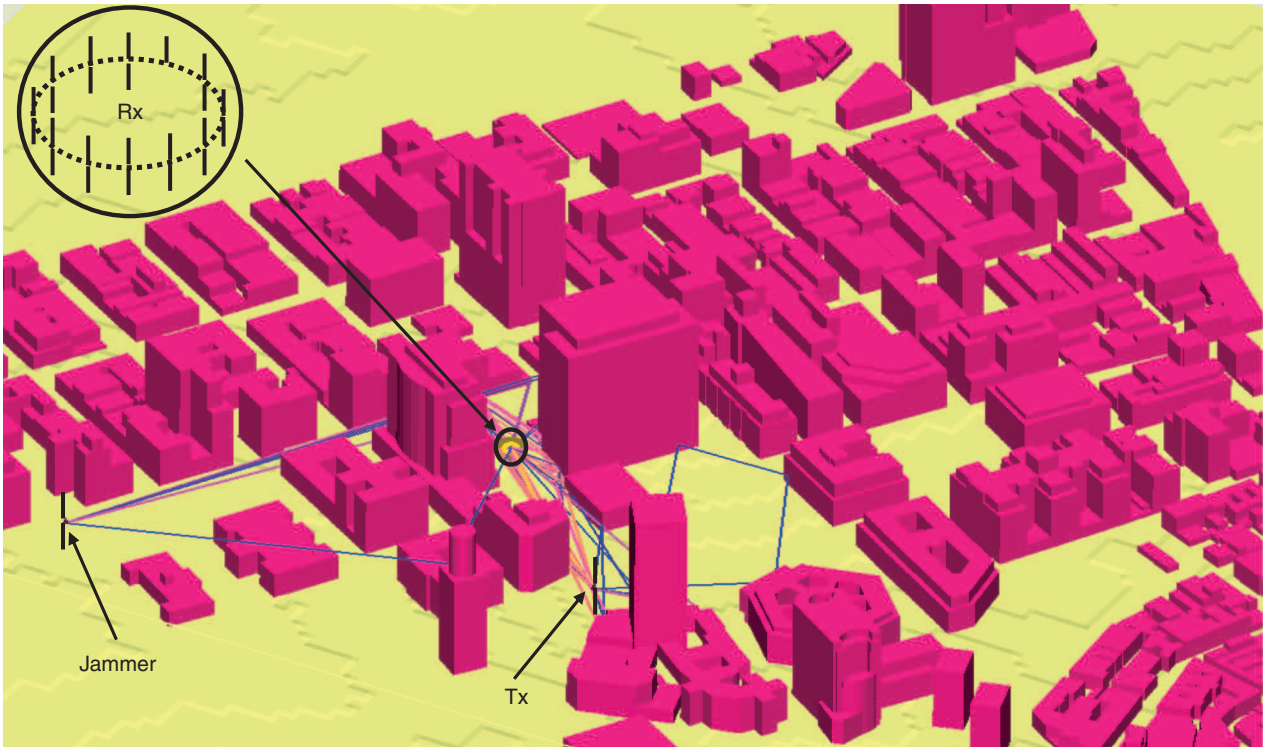

FIGURE 11. The ray-tracing simulation results obtained by the EM.Terrano simulator for a scenario in downtown Manhattan. A large number of rays arrive at the Rx array from both the communication Tx and the jammer.

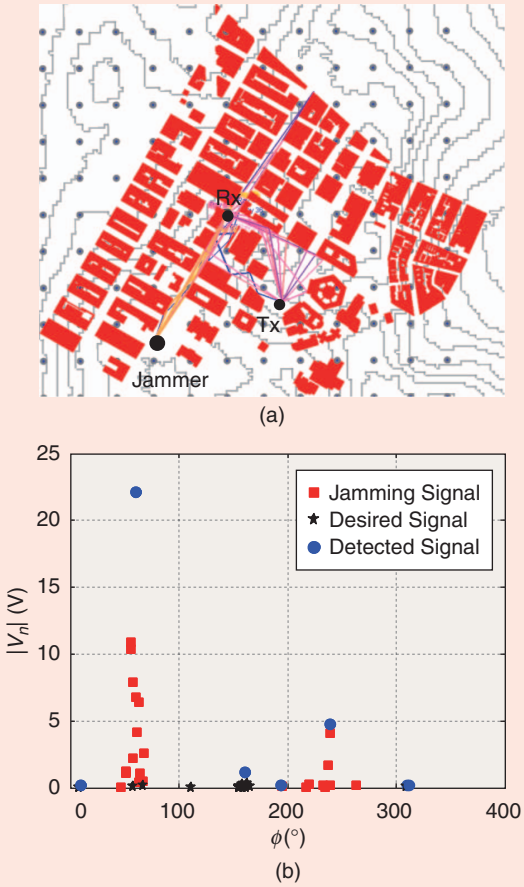

FIGURE 12. (a) An example scenario for HDR mode. (b) The detected signals (center frequency component) for this scenario.

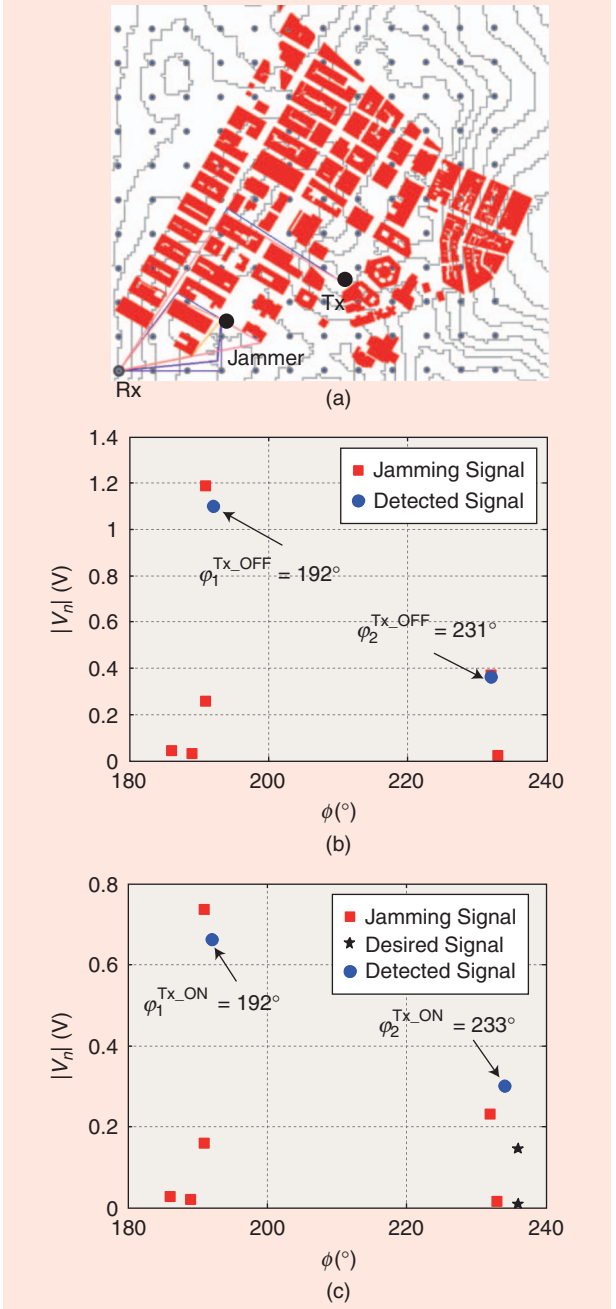

FIGURE 13. (a) An example scenario for LDR mode. (b) The detected signals (center frequency component) for this scenario when the Tx is off. (c) The detected signals (center frequency component) for this scenario when the Tx is on.

knowledge of the DoAs of the desired signals for maximizing the signal-to-interference ratio. Therefore, failure in the detection of the desired signals leads to the failure of the existing adaptive array techniques for interference cancelation. There are also situations in practice where many small signals from different DoAs arrive at the Rx with total power comparable to that of a larger signal, and if the algorithm cannot detect these small signals, the estimation of DoAs of the stronger signals will be erroneous.

In all simulations, it is assumed that the array is calibrated to capture the fabrication errors, and thereby the array manifold is perfectly known. It should be noted that imperfect estimation of the array manifold generally results in the performance degradation of ASSIA and in particular puts a lower limit in the DR of the signals that can be handled by ASSIA. The reason for the latter is that a relative small error in the estimation of the large signals generates a relatively large error in the estimation of the small signals. The DR of the signal that ASSIA can handle is reduced as the systematic errors increase. This problem is not, however, unique to ASSIA but applies to all other DoA estimators. Array calibration is essential to maximally benefit from the features that ASSIA offers.

PERFORMANCE ANALYSIS IN A COMPLEX ENVIRONMENT

To evaluate the performance of ASSIA under very complex and realistic conditions, a congested urban environment is considered. Such an environment is characterized as a Rayleigh fading environment. Downtown Manhattan, which is considered a complex wave propagation environment [56], is chosen as the simulation domain. A very fast and accurate urban wave propagation simulation software (EM.Terrano of the EM.Cube

package [57]) is used for broadband wave propagation simulation. Figure 11 illustrates the simulation scenario generated by EM.Terrano. The software allows placement of multiple Txs of arbitrary power level and arbitrary radiation pattern and provides the field coverage over the entire or a portion of the simulation area with desired resolution. For each point on the Rx grid, the software provides a vector containing the magnitude and phase of all rays arriving at that point with their corresponding angle of arrival. This information is used to assess the performance of the proposed algorithm. Choosing a Tx location and using it as jammer, the performance of the algorithm can also be evaluated in terms of its ability to segregate the desired signal. The area of the region illustrated in Figure 11 is 1,200 m × 1,200 m, within which one communication Tx, one jammer, and one Rx are placed at the antenna height of 2 m from the ground. The buildings are assumed to be impenetrable objects composed of brick with $\varepsilon_r = 4.44$. As before, the Rx is composed of a uniform circular array of 12 dipole antennas designed to operate at 300 MHz. The desired transmitted signal is assumed to have a bandwidth of 4 MHz from 298 to 302 MHz with binary phase-shift keying modulation, and the jamming signal is assumed to be a white Gaussian noise, each of which is radiated through omnidirectional antennas. It should be noted that because each frequency component of the signals is processed separately, ASSIA imposes no constraints on the waveform of the jamming signal. Therefore, if the jamming signal has any other waveform instead of white Gaussian noise or even is correlated with the desired signal, ASSIA is able to detect and separate all interfering and desired signals. The resolution of the FFT that is applied at the Rx baseband is 10 kHz. The Tx and the jammer power are adjusted so that, within the signal bandwidth, the SNR and SJR at the Rx are 20 and −20 dB, respectively. An example scenario for HDR mode is illustrated in Figure 12(a). As depicted in Figure 12(a), a large number of rays arrive at the Rx emanating from both the Tx and the jammer. For this scenario, as is evident from Figure 12(b), six DoAs are detected by the Rx. It is also shown that the jamming signals are arriving from three main separable directions and, for each main direction, there are many adjacent rays. The desired signal, on the other hand, is arriving at the Rx from five main separable directions, among which one overlaps with the jamming signal. The rays from this direction are not read as the desired signal. Also, one ray is not detected due to its low amplitude compared to the predetermined threshold level and the algorithm errors as well. These errors occur when the contribution of other signals is not subtracted perfectly because a large number of rays is arriving at the Rx within the azimuthal angular range from 150 to 250°, which

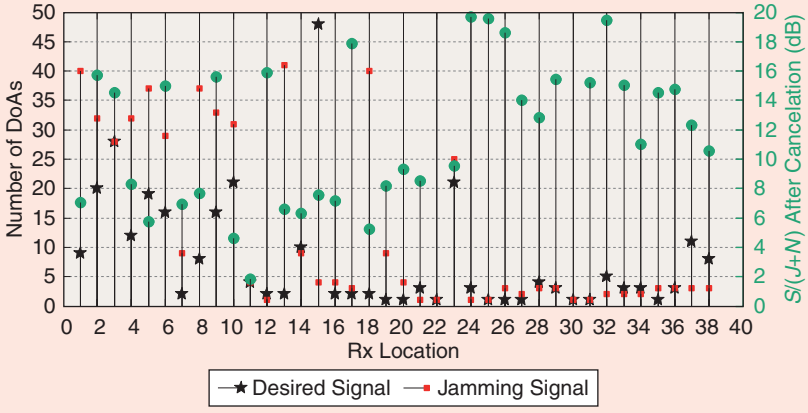

FIGURE 14. The number of DoAs of the desired (black pentagrams) and the jamming (red squares) signals and $S/(J+N)$ after mitigation (green circles) in HDR mode for 38 Rx locations.

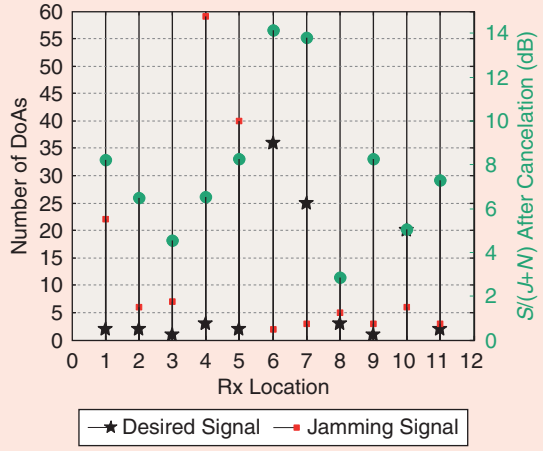

FIGURE 15. The number of DoAs of the desired (black pentagrams) and the jamming (red squares) signal and $S/(J+N)$ after mitigation (green circles) in LDR mode for 11 Rx locations.

are not far enough apart to be segregated and estimated by the algorithm accurately. Therefore, three desired and three jamming signals are detected, some of which represent the resultant of the adjacent arriving signals.

This procedure is done for all frequency components, and the jamming signals are subtracted from the total received signal at each antenna. Eventually, the cleaned-up signal from each antenna goes through further signal processing and decoding, which is not pertinent to this discussion. For this scenario, the achieved SJR after the cancelation procedure is 9.5 dB, which indicates 29.5-dB improvement. Now consider the scenario demonstrated in Figure 13(a), in which the desired and the jamming signals arrive at the Rx from nearby directions and a replica of the jamming signal quite away from the desired signal also exists. In this case, the Rx fails to retrieve the desired signal in HDR mode. Noting that SNR = 20 dB and SJR = −20 dB,

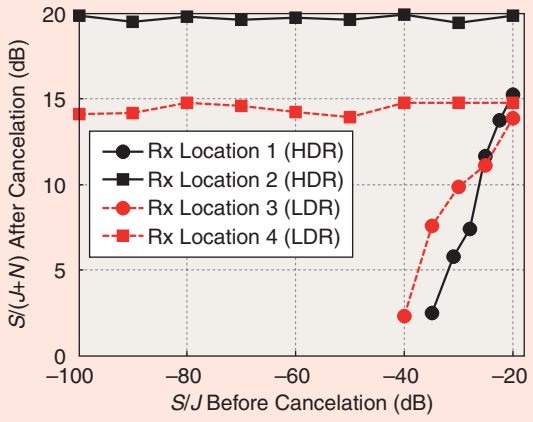

FIGURE 16. The $S/(J+N)$ after cancelation versus S/J before cancelation for four different Rx locations demonstrated in Figures 17 and 18.

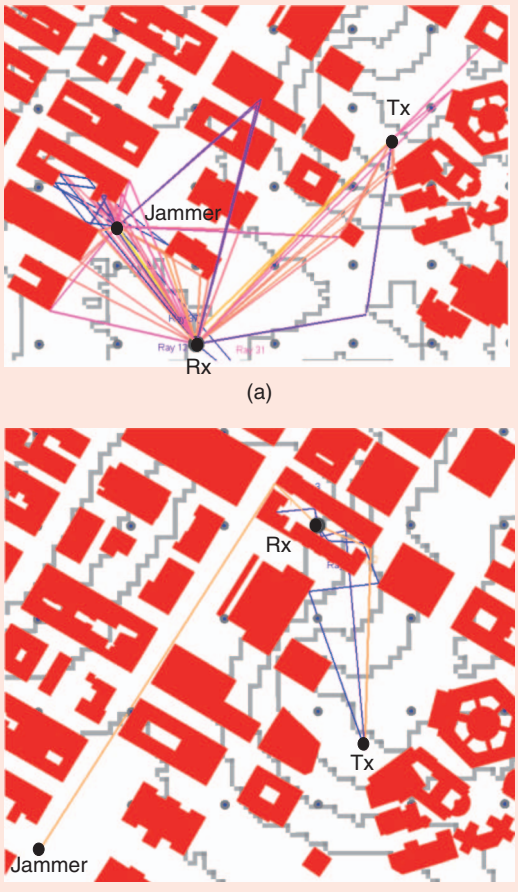

FIGURE 17. The sketch of the received rays for (a) Rx location 1 and (b) Rx location 2. The Rx operates in HDR mode in these locations.

Figure 13(b) and (c) shows the detected signals corresponding to the center frequency component in the Tx off state and the Tx on state, respectively. The detected DoAs for the jamming signal, which is close to the desired signal denoted as φ_2, change as the Tx transits from off state to on state. Based on the procedure described in the "Interference Segregation" section for LDR mode and assuming a perfect synchronization, which is beyond the scope of this article, the radio Rx will be able to make an estimation of the jamming signal from direction φ_2 and then clean up the received signal at each antenna. After jamming signal removal, the SJR is increased to +6.5 dB, which corresponds to 26.5-dB enhancement in this case.

The two previous examples clearly demonstrate the effectiveness of the ASSIA radio. However, a statistical analysis is carried out to show that the improvements observed are not accidental. For this purpose, 100 Rx locations are chosen randomly in the scene shown in Figure 11. The locations of the Tx and the jammer are kept the same for these series of simulations. For each Rx location, the power of the Tx and the jammer has been adjusted so that at the Rx point SNR = 20 dB and SJR = −20 dB. Out of 100 Rx locations, 30 points are not further examined, as either the signal or jammer was below the threshold. Out of 70 points at which the algorithm was tested, in 38 Rx locations, the radio has been able to effectively remove interference and boost the signal to jammer plus noise ratio (SJNR) to at least +2 dB (minimum of 22-dB improvement) in HDR mode. The number of DoAs of the desired and the jamming signals corresponding to each Rx location and $S/(J+N)$ after interference removal are illustrated on the same graph in Figure 14. The radio fails to retrieve the desired signal in HDR mode in other spots due to the proximity of the DoAs of the desired and the jamming signals. Switching to LDR mode enables the Rx to segregate the communication signal of interest from the interfering signal in 11 other locations. As shown in Figure 15, in the worst case, $S/(J+N)$ at the output of the ASSIA processor is higher than +2 dB. Therefore, the ASSIA radio succeeded in removing interference in a total of 49 out of 70 spots (70% of occasions) with better than 22-dB improvement. In 21 locations out of 70 points, the desired and the jamming signals all arrived with similar DoAs, for which even the LDR was challenged to cancel out the jammer substantially.

The success level can, of course, be improved significantly if we did not force SJR to be −20 at every location. Also by increasing the number of antennas and in turn reducing the array beamwidth, the performance of the radio can be enhanced. The number of DoAs of the desired and the jamming signals and their angular distance affect the enhancement level of $S/(J+N)$. Roughly, one can say that the lower the number of DoAs and the larger their angular distance, the higher the performance improvement.

Figure 16 illustrates the SJNR after cancelation versus SJR before cancelation by using the same Rx array in four different Rx locations. Two of these scenarios correspond to HDR mode, and the other two correspond to LDR mode shown in Figures 17 and 18, respectively. As before, it is assumed that SNR = 20 dB for these simulations. Figure 16

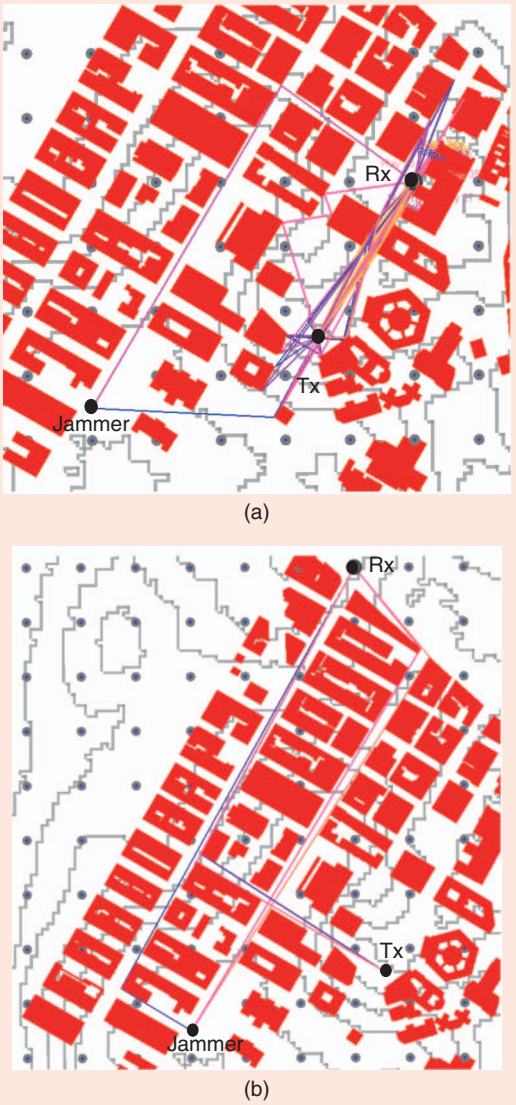

FIGURE 18. The sketch of the received rays for (a) Rx location 3 and (b) Rx location 4. The Rx operates in LDR mode in these locations.

further reveals that the performance of the radio depends on the scenario complexity, that is, the number of DoAs, their angular distance, and the SJR. The reason for better performance of the radio Rx in location 2 compared to location 1 for very low SJR in HDR mode pertains to the proximity of DoAs of the desired and jamming signals in location 1. The algorithm also exhibits excellent cancelation of the jamming signal in LDR mode in location 4, which is better than that for location 3 for very low SJR. This is due to the fact that, in location 4, there exist rays of jamming signals with DoAs that are apart from the desired signals and can be estimated accurately by the algorithm. In location 3, the jammer signal is not estimated as accurately as in location 4 due to there not being enough angular distance from the desired signals.

CONCLUSIONS

This article demonstrates an iterative algorithm for capturing the DoAs, magnitudes, and phases of all correlated or uncorrelated impinging signals on an Rx with angular spacing larger than the array beamwidth over a wide DR. This algorithm is implemented for a radio with a circular array of antennas, each of which is connected to a coherent Rx. It is shown that such a radio Rx is capable of suppressing interfering signals in complex multipath environments without a priori knowledge regarding the DoAs of the desired or interference signals. The proposed approach for interference cancelation is proved to be efficient using a statistical analysis in an urban environment with rich multipath propagation characteristics.

ACKNOWLEDGMENT

This research was supported by the Space and Terrestrial Communications Directorate of the U.S. Army Communications-Electronics Research, Development, and Engineering Center.

AUTHOR INFORMATION

S. Mohammad Amjadi (smamjadi@umich.edu) is currently pursuing his Ph.D. degree in electrical and electronics engineering from the University of Michigan, Ann Arbor. His research interests include the areas of antennas, multiple-antenna communication systems, and interference cancelation in complex multipath environments.

Mahbub Hoque (Mahbub.Hoque1@us.army.mil) is the chief of international programs and global technology research in the U.S. Army's Communications-Electronics Research, Development, and Engineering Center, Aberdeen Proving Ground, Maryland. He has led numerous programs for developing antennas for Army applications and radio-frequency modeling and simulation techniques for analyzing interference on combat platforms.

Kamal Sarabandi (saraband@umich.edu) is the Rufus S. Teesdale endowed professor of engineering and director of the Radiation Laboratory at the University of Michigan, Ann Arbor. His research areas of interest include microwave and millimeter-wave radar remote sensing, metamaterials, electromagnetic wave propagation, and antenna miniaturization.

REFERENCES

[1] P. W. Howells, "Intermediate frequency side-lobe canceller," U.S. Patent 3 202 990 A, Aug. 24, 1965.

[2] S. P. Applebaum, "Adaptive arrays," *IEEE Trans. Antennas Propag.*, vol. 24, no. 5, pp. 585–598, Sept. 1976.

[3] B. D. Van Veen, "Eigenstructure based partially adaptive array design," *IEEE Trans. Antennas Propag.*, vol. 36, pp. 357–362, Mar. 1988.

[4] A. M. Haimovich and Y. Bar-Ness, "An eigenanalysis interference canceler," *IEEE Trans. Signal Process.*, vol. 39, pp. 76–84, Jan. 1991.

[5] W. S. Youn and C. K. Un, "Robust adaptive beamforming based on the eigenstructure method," *IEEE Trans. Signal Process.*, vol. 42, pp. 1543–1547, June 1994.

[6] J. L. Yu and C. C. Yeh, "Generalized eigenspace-based beamformers," *IEEE Trans. Signal Process.*, vol. 43, pp. 2453–2461, Nov. 1995.

[7] A. Klouche-Djedid and M. Fujita, "Adaptive array sensor processing applications for mobile telephone communications," *IEEE Trans. Veh. Technol.*, vol. 45, no. 3, pp. 405–416, Aug. 1996.

[8] A. Ranheim, "A decoupled approach to adaptive signal separation using an antenna array," *IEEE Trans. Veh. Technol.*, vol. 48, no. 3, pp. 676–682, May 1999.

[9] T. K. Sarkar, J. Koh, R. Adve, R. A. Schneible, M. C. Wicks, S. Choi, and M. Salazar-Palma, "A pragmatic approach to adaptive antennas," *IEEE Antennas Propag. Mag.*, vol. 42, no. 2, pp. 39–55, Apr. 2000.

[10] J. H. Lee and C. C. Lee, "Analysis of the performance and sensitivity of an eigenspace-based interference canceler," *IEEE Trans. Antennas Propag.*, vol. 48, pp. 826–835, May 2000.

[11] O. L. Frost III, "An algorithm for linearly constrained adaptive array processing," *Proc. IEEE*, vol. 60, no. 8, pp. 926–935, Aug. 1972.

[12] B. Widrow, K. M. Duvall, R. P. Gooch, and W. C. Newman, "Signal cancellation phenomena in adaptive antennas: Causes and cures," *IEEE Trans. Antennas Propag.*, vol. 30, pp. 469–478, May 1982.

[13] A. Luthra, "Maximum entropy method in the space-angle domain and a new technique with superior performance," Ph.D. dissertation, Dept. Syst. Eng., Univ. Pennsylvania, Philadelphia, 1981.

[14] J. E. Evans, J. R. Johnson, and D. F. Sun, "Application of advanced signal processing techniques to angle of arrival estimation in ATC navigation and surveillance system," Lincoln Lab., Massachusetts Inst. of Technology, Cambridge, Lincoln Lab. Tech. Rep. 582, 1982.

[15] T. J. Shan and T. Kailath, "Adaptive beamforming for coherent signals and interference," *IEEE Trans. Acoust., Speech, Signal Process.*, vol. 33, no. 3, pp. 527–536, June 1985.

[16] A. K. Luthra, "A solution to the adaptive nulling problem with a look-direction constraint in the presence of coherent jammers," *IEEE Trans. Antennas Propag.*, vol. 34, no. 5, pp. 702–710, May 1986.

[17] R. O. Schmidt, "Multiple emitter location and signal parameter estimation," *IEEE Trans. Antennas Propag.*, vol. 34, no. 3, pp. 276–280, Mar. 1986.

[18] A. J. Barabell, "Improving the resolution performance of eigenstructure-based direction-finding algorithms," in *Proc. IEEE Int. Conf. Acoustics, Speech, and Signal Processing*, Boston, MA, 1983, pp. 336–339.

[19] M. D. Zoltowski, G. M. Kautz, and S. D. Silverstein, "Beamspace ROOT-MUSIC," *IEEE Trans. Signal Process.*, vol. 41, no. 1, pp. 344–364, Feb. 1993.

[20] E. Falletti, L. Lo Presti, and F. Sellone, "SAM LOST smart antennas-based movable localization system," *IEEE Trans. Veh. Technol.*, vol. 55, no. 1, pp. 25–42, Jan. 2006.

[21] Y. Y. Wang, L. C. Lee, S. J. Yang, and J. T. Chen, "A tree structure one-dimensional based algorithm for estimating the two-dimensional direction of arrivals and its performance analysis," *IEEE Trans. Antennas Propag.*, vol. 56, no. 1, pp. 178–188, Jan. 2008.

[22] A. Hirota, H. Arai, and M. Nakano, "Direction-of-arrival estimation system for multipath propagation in code-division multiple-access systems with synthesized virtual planar array using pilot signals," *IEEE Trans. Veh. Technol.*, vol. 57, no. 4, pp. 2153–2163, July 2008.

[23] G. Hislop, N. Sakar, and C. Craeye, "Direction finding with MUSIC and CLEAN," *IEEE Trans. Antennas Propag.*, vol. 61, no. 7, pp. 3839–3849, July 2013.

[24] W. J. Zeng, H. C. So, and H. Lei, "l_p-MUSIC: Robust direction-of-arrival estimator for impulsive noise environments," *IEEE Trans. Signal Process.*, vol. 61, no. 17, pp. 4296–4308, Sept. 2013.

[25] R. Roy and T. Kailath, "ESPRIT-estimation of signal parameters via rotational invariance techniques," *IEEE Trans. Acoust., Speech, Signal Process.*, vol. 37, no. 7, pp. 984–995, July 1989.

[26] M. Haardt, *Efficient One-, Two-, and Multidimensional High-Resolution Array Signal Processing*. New York: Shaker Verlag, 1997.

[27] M. D. Zoltowski, M. Haardt, and C. P. Mathews, "Closed-form 2-D angle estimation with rectangular arrays in element space or beamspace via unitary ESPRIT," *IEEE Trans. Signal Process.*, vol. 44, pp. 316–328, Feb. 1996.

[28] G. Xu, S. D. Silverstein, R. H. Roy, and T. Kailath, "Beamspace ESPRIT," *IEEE Trans. Signal Process.*, vol. 42, no. 2, pp. 349–356, Feb. 1994.

[29] M. Haardt and J. A. Nossek, "Unitary ESPRIT: How to obtain increased estimation accuracy with a reduced computational burden," *IEEE Trans. Signal Process.*, vol. 43, pp. 1232–1242, May 1995.

[30] J. J. Blanz, A. Papathanassiou, M. Haardt, L. Furio, and P. W. Baier, "Smart antennas for combined DOA and joint channel estimation in time-slotted CDMA mobile radio systems with joint detection," *IEEE Trans. Veh. Technol.*, vol. 49, no. 2, pp. 293–306, Mar. 2000.

[31] T. J. Shan and T. Kailath, "On spatial smoothing for direction-of-arrival estimation of coherent signals," *IEEE Trans. Acoust., Speech, Signal Process.*, vol. 33, no. 4, pp. 806–811, Aug. 1985.

[32] R. T. Williams, S. Prasad, A. K. Mahalanabis, and L. H. Sibul, "An improved spatial smoothing technique for bearing estimation in a multipath environment," *IEEE Trans. Acoust., Speech, Signal Process.*, vol. 36, pp. 425–432, Apr. 1988.

[33] S. U. Pillai and B. H. Kwon, "Forward/backward spatial smoothing techniques for coherent signal identification," *IEEE Trans. Acoust., Speech, Signal Process.*, vol. 37, pp. 8–15, Jan. 1989.

[34] M. Wax and J. Sheinvald, "Direction finding of coherent signals via spatial smoothing for uniform circular arrays," *IEEE Trans. Antennas Propag.*, vol. 42, no. 5, pp. 613–620, May 1994.

[35] P. S. Chang and A. L. Wilson, "Conjugate gradient method for adaptive direction-of-arrival estimation of coherent signals," in *Proc. IEEE Int. Conf. Acoustics, Speech, and Signal Processing (ICASSP)*, 1997, pp. 2281–2284.

[36] E. Gonen, J. M. Mendel, and M. C. Dogan, "Applications of cumulants to array processing. IV. Direction finding in coherent signals case," *IEEE Trans. Signal Process.*, vol. 45, no. 9, pp. 2265–2276, Sept. 1997.

[37] T. K. Sarkar and O. Pereira, "Using the matrix pencil method to estimate the parameters of a sum of complex exponentials," *IEEE Antennas Propag. Mag.*, vol. 37, no. 1, pp. 48–55, Feb. 1995.

[38] N. Yilmazer, J. Koh, and T. K. Sarkar, "Utilization of a unitary transform for efficient computation in the matrix pencil method to find the direction of arrival," *IEEE Trans. Antennas Propag.*, vol. 54, no. 1, pp. 175–181, Jan. 2006.

[39] J. Rissanen, "Modeling by the shortest data description," *Automatica*, vol. 14, pp. 465–471, 1978.

[40] H. Akaike, "Information theory and extension of the maximum likelihood principle," in *Proc. 2nd Int. Symp. Information Theory*, 1973, pp. 267–281.

[41] M. Wax and T. Kailath, "Detection of signals by information theoretic criterion," *IEEE Trans. Acoust., Speech, Signal Process.*, vol. 33, no. 2, pp. 387–392, Apr. 1985.

[42] R. Bachl, "The forward–backward averaging technique applied to TLS-ESPRIT processing," *IEEE Trans. Signal Process.*, vol. 43, no. 11, pp. 2691–2699, Nov. 1995.

[43] J. Capon, "High-resolution frequency-wavenumber spectrum analyses," *Proc. IEEE*, vol. 57, no. 8, pp. 1408–1418, Aug. 1969.

[44] D. H. Johnson, "The application of spectral estimation methods to bearing estimation problems," *Proc. IEEE*, vol. 70, no. 9, pp. 1018–1028, Sept. 1982.

[45] I. Ziskind and M. Wax, "Maximum likelihood localization of multiple sources by alternating projection," *IEEE Trans. Acoust., Speech, Signal Process.*, vol. 36, pp. 1560–1577, Oct. 1988.

[46] M. Pesavento and A. B. Gershman, "Maximum-likelihood direction-of-arrival estimation in the presence of unknown nonuniform noise," *IEEE Trans. Signal Process.*, vol. 49, no. 7, pp. 1310–1324, July 2001.

[47] X. Wang and Z. X. Wang, "The estimation of the directions of arrival of the spread-spectrum signals with three orthogonal sensors," *IEEE Trans. Veh. Technol.*, vol. 51, no. 5, pp. 817–822, Sept. 2002.

[48] S. Marano, V. Matta, P. Willett, and L. Tong, "Support-based and ML approaches to DOA estimation in a dumb sensor network," *IEEE Trans. Signal Process.*, vol. 54, no. 4, pp. 1563–1567, Apr. 2006.

[49] O. Hernandez, F. Bouchereau, and D. Munoz, "Maximum likelihood position estimation in ad-hoc networks using a dead reckoning approach," *IEEE Trans. Wireless Commun.*, vol. 7, no. 5, pp. 1572–1584, May 2008.

[50] Z. M. Liu, Z. T. Huang, and Y. Y. Zhou, "An efficient maximum likelihood method for direction-of-arrival estimation via sparse Bayesian learning," *IEEE Trans. Wireless Commun.*, vol. 11, no. 10, pp. 1–11, Oct. 2012.

[51] G. Wang, Y. Li, and N. Ansari, "A semidefinite relaxation method for source localization using TDOA and FDOA measurements," *IEEE Trans. Veh. Technol.*, vol. 62, no. 2, pp. 853–862, Feb. 2013.

[52] S. M. Amjadi and K. Sarabandi, "Mutual coupling mitigation in broadband multiple-antenna communication systems using feedforward technique," *IEEE Trans. Antennas Propag.*, vol. 64, no. 5, pp. 1642–1652, May 2016.

[53] B. K. Lau and Y. H. Leung, "A Dolph–Chebyshev approach to the synthesis of array patterns for uniform circular arrays," in *Proc. 2000 IEEE Int. Symp. Circuits and Systems (ISCAS)*, pp. 124–127.

[54] M. P. Daly, E. L. Daly, and J. T. Bernhard, "Demonstration of directional modulation using a phased array," *IEEE Trans. Antennas Propag.*, vol. 58, no. 5, pp. 1545–1550, May 2010.

[55] A. Babakhani, D. B. Rutledge, and A. Hajimiri, "Transmitter architectures based on near-field direct antenna modulation," *IEEE J. Solid-State Circuits*, vol. 43, no. 12, pp. 2674–2692, Dec. 2008.

[56] D. Chizhik, J. Ling, P. W. Wolniansky, R. A. Valenzuela, N. Costa, and K. Huber, "Multiple-input–multiple-output measurements and modeling in Manhattan," *IEEE J. Sel. Areas Commun.*, vol. 21, no. 3, pp. 321–331, Apr. 2003.

[57] EMAG Technologies Inc. (2014). EM.Cube. EMAG Technologies Inc. Ann Arbor, MI. [Online]. Available: http://www.emagtech.com/content/emcube